REPORT DOCUMENTATION PAGE

Form Approved
OMB No. 0704-0188

1. REPORT DATE *(DD-MM-YYYY)*	**2. REPORT TYPE**	**3. DATES COVERED** *(From - To)*
14-12-2010	Article	DEC 2010 - JAN 2011

4. TITLE AND SUBTITLE

A Portable Thermoelectric Power Generator Based on a Microfabricated Silicon Combustor with Low Resistance to Flow

5a. CONTRACT NUMBER
FA8720-05-C-0002

5b. GRANT NUMBER

5c. PROGRAM ELEMENT NUMBER

6. AUTHOR(S)

C.R. Marton, G.S. Haldeman, and K.F. Jensen

5d. PROJECT NUMBER

5e. TASK NUMBER

5f. WORK UNIT NUMBER

7. PERFORMING ORGANIZATION NAME(S) AND ADDRESS(ES)

MIT Lincoln Laboratory
244 Wood Street
Lexington, MA 02420

8. PERFORMING ORGANIZATION REPORT NUMBER

9. SPONSORING / MONITORING AGENCY NAME(S) AND ADDRESS(ES)

ESC/CAA
20 Schilling Circle, Bldg 1305
Hanscom AFB, MA 01731

10. SPONSOR/MONITOR'S ACRONYM(S)

ESC/CAA

11. SPONSOR/MONITOR'S REPORT NUMBER(S)

12. DISTRIBUTION / AVAILABILITY STATEMENT

DISTRIBUTION STATEMENT A. Approved for public release; distribution is unlimited.

13. SUPPLEMENTARY NOTES

14. ABSTRACT

A portable-scale thermoelectric power generator was designed, fabricated, and tested. The basis of the system is a mesoscale silicon reactor for the combustion of butane over an alumina-supported platinum catalyst. The system is integrated with commercial bismuth telluride thermoelectric modules to produce 5.8 W of electrical power with a chemical-to-electrical conversion efficiency of 2.5% (based on LHV). The energy and power densities of the demonstrated system are 321 W h kg-1 and 17 W kg-1, respectively. The pressure drop through the system is 130 Pa for the highest now rate used, resulting in a parasitic power requirement for air-pressurization of ~0.1 W. The demonstration represents an order-of-magnitude improvement in portable-scale electrical power from thermoelectrics and hydrocarbon fuels, and a notable increase in the conversion efficiency compared with previous studies.

15. SUBJECT TERMS

16. SECURITY CLASSIFICATION OF:			**17. LIMITATION OF ABSTRACT**	**18. NUMBER OF PAGES**	**19a. NAME OF RESPONSIBLE PERSON**
U					Zach Sweet
a. REPORT	**b. ABSTRACT**	**c. THIS PAGE**	SAR	11	**19b. TELEPHONE NUMBER** *(include area code)*
U	U	U			781-981-5997

Standard Form 298 (Rev. 8-98)
Prescribed by ANSI Std. Z39.18

JA-17945

A Portable Thermoelectric Power Generator Based on a Microfabricated Silicon Combustor with Low Resistance to Flow

C.H. Marton[a], G.S. Haldeman[b], K.F. Jensen[a,*]

a *Department of Chemical Engineering, Massachusetts Institute of Technology, 77 Massachusetts Avenue, Cambridge, MA 02139, USA.*
b *Lincoln Laboratory, Massachusetts Institute of Technology, 244 Wood Street, Lexington, MA 02420, USA.*
**Corresponding author. Fax: 617-258-8992. Email kfjensen@mit.edu*

Abstract
A portable-scale thermoelectric power generator was designed, fabricated, and tested. The basis of the system is a mesoscale silicon reactor for the combustion of butane over an alumina-supported platinum catalyst. The system is integrated with commercial bismuth telluride thermoelectric modules to produce 5.8 W of electrical power with a chemical-to-electrical conversion efficiency of 2.5% (based on LHV). The energy and power densities of the demonstrated system are 321 W h kg^{-1} and 17 W kg^{-1}, respectively. The pressure drop through the system is 130 Pa for the highest flow rate used, resulting in a parasitic power requirement for air-pressurization of ~0.1 W. The demonstration represents an order-of-magnitude improvement in portable-scale electrical power from thermoelectrics and hydrocarbon fuels, and a notable increase in the conversion efficiency compared with previous studies.

1. Introduction

The energy densities of many hydrocarbon fuels exceed those of conventional batteries by several orders of magnitude. For example, the lower heating value of n-butane is 12700 W h kg^{-1}, compared with 150 – 300 W h kg^{-1} for lithium-ion cells [1]. This gap, as well as the potential for instantaneous recharging and reduced environmental impact [2], motivates research efforts into alternative portable power generation devices based on hydrocarbon fuels. Light hydrocarbons, such as butane, are attractive sources for portable power generation because they can be stored as a liquid under modest pressure (allowing for possible storage in plastic or thin metals). Additionally, the vapor pressure of the fuel could be used to eliminate the need for a fuel pump. Typical portable power generation strategies based on hydrocarbons include combustion-based approaches such as miniature engines [3, 4], thermophotovoltaic conversion of radiated photons [5], or thermoelectric conversion [6], as well as direct [7] or indirect [8] conversion in a fuel cell.

Thermoelectric (TE) power generation utilizes the Seebeck effect to generate electricity from a temperature difference maintained between two areas bridged by thermoelectric materials. An electrical potential difference develops across the TE materials as a result of charge carrier diffusion from the hot to the cold side, and this potential can be used to drive a useful load with many elements connected thermally in parallel and electrically in series. The principles of TE power generation are described in detail by Rowe [9]. TE power generation is an attractive option for portable devices because it offers a direct, passive conversion of heat to electricity that is quiet and generates only CO_2 and water. The generation system consists of a heat source such as a combustor, a cold region connected to either a passive or active cooling system, and the appropriate TE materials (e.g., solid solutions such as BiTe, PbTe, SiGe) connecting the two temperature zones. Recently, TE power generation with thermal-to-electrical energy conversion efficiency of 8% was demonstrated with a temperature difference (from hot to cold side) of 400°C using cascaded BiTe TE modules [10].

Compared with fuel cells or other combustion-based systems, thermoelectric (TE) power generators are desirable due to the high power densities that can be achieved. For example, Venkatasubramanian, et al., have estimated the power density (flux) of their thin-film TE material at 700 W cm^{-2} [11]. TE power generation is also attractive for portable systems due to the low temperatures which may be used, which result in a reduced heat signature for military applications and reduced safety concerns for consumer devices compared with other combustion-based systems. Commercial bismuth telluride-based TE modules are often limited to temperatures below

300°C. Catalytic combustion is particularly well suited for TE power generation because of this relatively low temperature ceiling.

There are many examples of micro- and mesoscale thermoelectric power generators powered by catalytic combustion in the literature. Cohen, et al., patented an integrated TE device based on a ceramic "Swiss-roll" structure [12]. Vican, et al., also developed a TE power generation system based on an alumina ceramic "Swiss-roll" using a stereolithography process; however, the maximum power output reported from this system was 52 mW from a hydrogen input of 9.1 W equivalent [13]. A TE generator fabricated from silicon bonded to glass was developed by Yoshida, et al., but the high heat loss from the device prevented the autothermal combustion of butane [14]. The device was able to produce 184 mW of electrical power with an efficiency of 2.8% from the catalytic combustion of hydrogen.

Perhaps the most significant recent effort directed towards the design and understanding of an integrated combustor-TE power generator has come from the Vlachos group at the University of Delaware. Their stainless steel device has been used to combust hydrogen, propane [6, 15, 16], and methanol [17]. The combustor was integrated with a commercial BiTe-based TE device from Hi-Z Technology, Inc. The group has reported the production of 1 W maximum power and a thermal-to-electrical conversion efficiency of 1.08% with hydrogen as the fuel, with energy and power densities of 67 Wh/kg and 5 W/kg, respectively. The group has also reported the generation of 0.45 W electrical power with propane as the fuel at 0.66% conversion efficiency. The group reported 0.65 W power generated from methanol combustion, and claim that the 1.1% conversion efficiency is the highest reported for TE power generation using a liquid fuel. The demonstration of a fuel-based TE generator suitable for portable power with energy density comparable to that of a battery remains an open challenge.

In this work, a portable-scale power generation system was developed based on the catalytic combustion of n-butane within a silicon mesoreactor, commercially-available TE modules, and air-cooled heat sinks. The system was designed for low flow resistance, such that the parasitic power requirement for air-pressurization would comprise a small fraction of the total power produced.

2. System Design

2.1 Design Concepts

As the length scales of a system decrease (from m to mm, and further to μm), the ratio of surface area to volume increases, and it is increasingly difficult to design a small, thermally isolated high-temperature system. The heat generation rate scales with the internal volume, while the heat transfer rates, both for useful transfer to the TE modules and for heat loss, scale with external surface area. The steady state

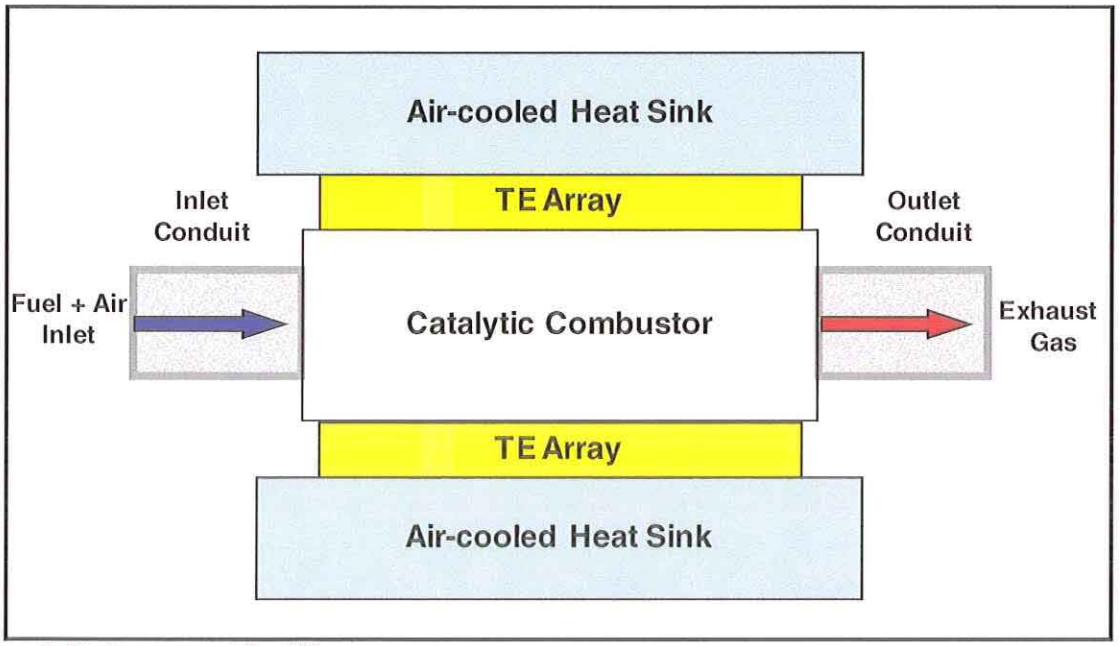

Figure 1: Design concept for TE power generator.

temperature profile and the thermal efficiency of a combustor are determined by the comparison of heat generation in the reactor and heat loss pathways. Achieving the necessary thermal isolation is one of the most significant challenges in achieving high thermal efficiency in small scale devices [18].

The general design concept for this TE generator system is shown in Figure 1. The catalytic combustion of fuel provides heat to two TE modules, which sandwich the combustor. The opposite sides of the TE modules are air-cooled to create a large temperature gradient across the modules. The sandwiched-reactor configuration is conducive to good thermal management of the high-temperature system. The heat transfer from the system can be considered as five pathways: conductive and Peltier heat transfer through the TE modules, convective heat losses to the atmosphere, conductive heat loss through the fluidic conduits, radiative loss to the surroundings, and enthalpic loss to the heated exhaust stream. The sandwiched-reactor design concept greatly reduces the surface area exposed to the environment for convective and radiative heat transfer relative to the area for transfer to the TE modules.

Most portable power generation devices are intended to be air-breathing, that is, they are operated using air from the surrounding environment as the oxidant. As such, they incorporate some system to force air through the device (e.g., a fan or an ejector nozzle), which can serve as a parasitic load on the generated power or system mass. The energy required to provide air flow must be considered when designing an air-breathing fuel processor. The alternative would be to carry a volume of compressed oxidant, which has significant implications for system mass and volume.

For ejector nozzle systems, the combustor pressure drop must be very low in order to ensure that the vapor pressure of the fuel is sufficient to entrain sufficient air for combustion. Satoh, et al., developed a micro-ejector for use with butane in a TE power generator system, but found that it was limited to provide a system pressure of 31 Pa to achieve an equivalence ratio less than 1 [19]. For systems that use a fan or compressor to supply a forced stream of air, the flow work which must be provided is equal to the product of the volumetric flow rate and the system pressure drop. The parasitic power requirement for a fan or compressor is at least as much as the flow work divided by the fractional efficiency of the pressurization equipment. In this work, an estimated efficiency of 10% for a fan was used to assess the impact of the system pressure drop.

Examples of micro- and mesoscale catalytic combustors based on a number of different materials of construction (and fabrication processes) can be found in the literature. Silicon-based combustors have been developed using both reactive ion etch [20-22] and wet chemical etch [14, 23-25] techniques. Steel [14, 16, 23-27] and ceramic [13, 28] combustors have also been investigated. The choice of construction materials has a significant impact on combustor performance. It has been demonstrated that materials with higher thermal conductivity, such as silicon, can improve stability and enhance catalytic combustion relative to homogeneous combustion [29], as well as reduce thermal gradients that can occur within exothermic catalytic reactors [16, 30, 31]. However, materials with low thermal conductivity can reduce heat loss to the environment and allow for enthalpy recovery within the device [12, 28]. The integration of dissimilar materials has been demonstrated to lead to highly-thermally-efficient microcombustors [20, 21]; however, incorporating materials with dissimilar coefficients of thermal expansion in a device intended for use over a wide temperature range is no simple task. In this work, a silicon combustion zone was integrated with steel fluidic conduits.

2.2 *Combustor Design and Fabrication*

The layout of the combustor has been chosen in order to provide sufficient catalyst area to combust butane in the approximate flow range of 100 – 200 standard cubic centimeters per minute (sccm), while maintaining a low system pressure drop and limiting the heat loss from the system. The combustor has external dimensions of 35 x 28.5 x 4 mm^3, and is made from crystalline silicon. The TE junctions are arranged on the two large surfaces (35 x 28.5 mm^2), and the fluidic connections are made to the two 4 x 28.5 mm^2 faces. This design results in less than 280 mm^2 exposed to the atmosphere, which limits the convective and radiative heat loss without the use of vacuum packaging or radiation shields. The total mass of the catalyst-loaded silicon reactor was less than 5.5 g.

The combustor resembles a monolithic reactor (such as the cordierite monolith used by Moreno, et al. [32]), and consists of two stacked reactors, each made from two 1-mm-thick silicon wafers. There are 24 flow channels per reactor, each consisting of an open rectangle 35 mm in length. The selection of channel layout and dimensions, which are shown in Figure 2a and b, was influenced by the relationship

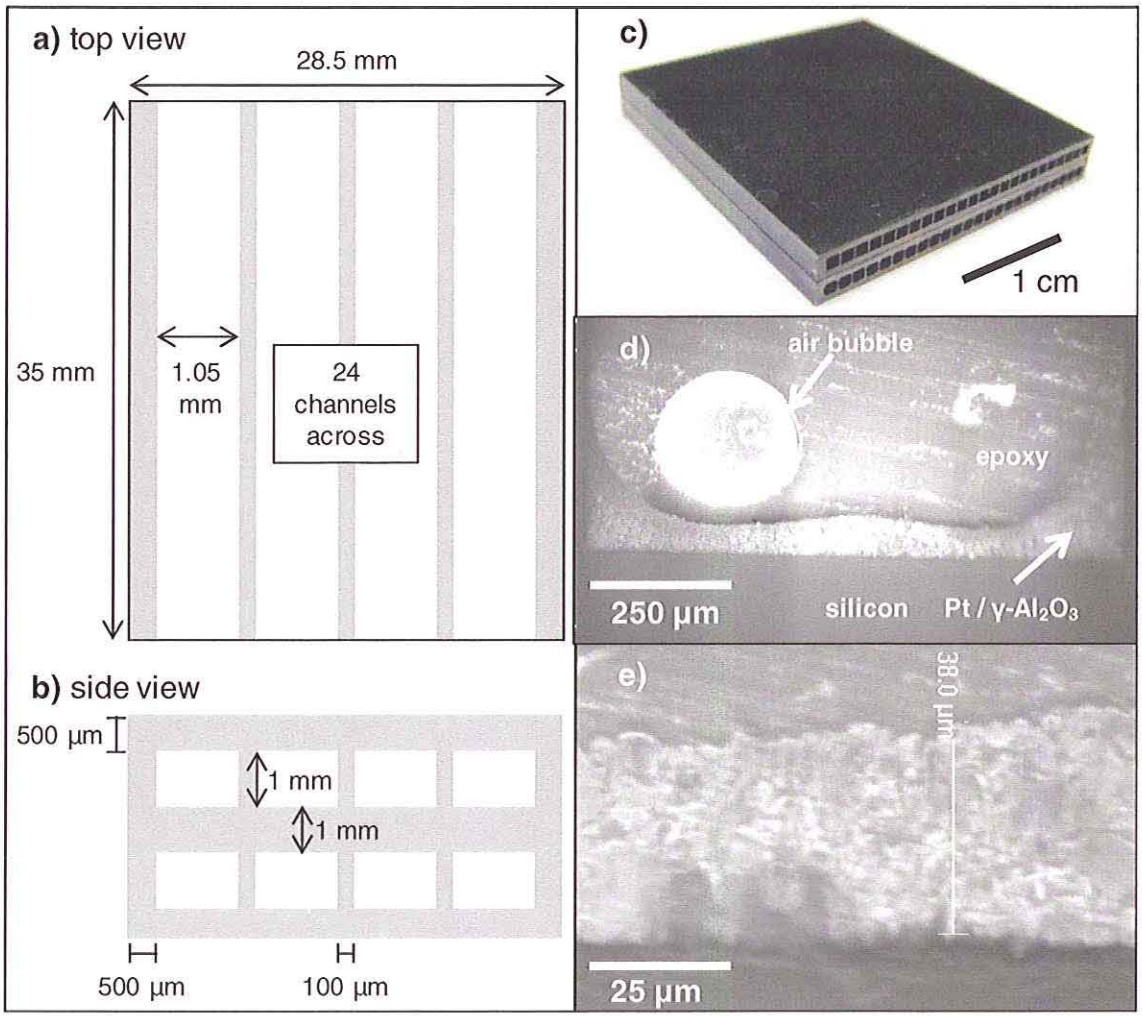

Figure 2: a) Top view of layout of reactor (not to scale). Only 4 of 24 channels are shown. Actual dimensions as labeled. b) Side view of reactor layout. c) Image of stacked combustor. d) Environmental SEM of platinum catalyst layer over an entire channel bottom. Note large feature is an air bubble in epoxy. e) Environmental SEM showing closer view of Pt alumina catalyst layer on bottom of channel.

between (internal) surface area of the exposed silicon (for catalyst deposition) and pressure drop through the channels. The pressure drop was modeled as laminar flow of an ideal gas in a rectangular channel using the Darcy-Weisbach equation. The hydraulic diameter of a rectangular channel is dominated by the smaller of the height of the channel (considered fixed at 1 mm) and the width of the channel (which is a function of the number of walls used to divide the internal chamber). Nearly square channels (1.05 mm wide and 1 mm high) were chosen to balance the desires for large internal surface area and low pressure drop. The thickness of the walls separating the channels was only 100 µm, and so considerable open frontal area was available.

The reactors were formed from 1-mm-thick, 6-in-diameter, double-sided polished n-type (100)-silicon wafers (James River Semiconductor). A protective layer of silicon dioxide was grown on the silicon wafers at a thickness of 400 nm, and on top of the oxide 400 nm of silicon-rich silicon nitride was deposited using low pressure chemical vapor deposition to serve as an etch mask. Channel-defining features and other alignment marks were defined in the etch mask using contact photolithography and subsequent reactive ion etch (to remove the silicon nitride) and buffered hydrofluoric acid etch (to remove the silicon oxide) steps. The channel-defining features consisted of arrays of 24 rectangles (each 50 µm by 96 mm) which were aligned to the <100> crystal plane. Rectangular half-channels (500 µm deep by 1050 µm wide) were

etched in each wafer using a 25% (by weight) potassium hydroxide bath at 80°C, with vertical side walls achieved as a result of the orientation to the crystal plane. After etching, the silicon nitride was removed in a bath of phosphoric acid at 165°C, and silicon oxide was removed using 49% hydrofluoric acid. The reaction channels were then enclosed using silicon fusion bonding [33]. The combustor was formed from two, two-wafer-reactors after dicing, as shown in Figure 2c. The use of a wet etch technique significantly reduces the fabrication cost of the reactor, and allows for a highly parallelized fabrication process (with multiple reactors per wafer, and simultaneous processing of wafers).

The combustor has a total internal surface area (for catalyst deposition) of 68.9 cm^2 and an internal volume of 1.76 cm^3. Because of the small surface area that is exposed to the environment, the addition of a second reactor does not significantly increase the system heat loss, while doubling the internal volume, for a fixed TE-module area. The use of two stacked reactors also allows for the relatively simple implementation of counter-current reaction channels, with the channel inlets of one reactor directly opposite the outlets of the other reactor. This configuration helps to improve the thermal uniformity of the system without the need for a complicated gas distribution system. The intention, confirmed by three-dimensional CFD simulation, is that the hot spot at the inlet of one set of channels would provide heat to the colder portion of the other set of channels, which are separated by only 1 mm of silicon. The relatively high thermal conductivity of silicon also helped to reduce thermal gradients.

The combustion catalyst was 5% (by weight) platinum supported on gamma-alumina (Sigma Aldrich). Wet catalyst powder was ground in a mortar for approximately one hour, which reduced the mean particle size to from 12.5 to 3.6 μm, as measured by laser diffraction (Malvern Mastersizer 2000). The prepared slurry contained 15% (by weight) solids in deionized water, and included a colloidal alumina suspension (Nyacol) at 1% (by weight) of total solids to increase adhesion to the silicon. To coat the channels, a process based on the general washcoating procedure for ceramic monoliths was used [34]. The slurry was first injected into the reactor channels using a syringe and the reactor was then "rested" horizontally for 5 minutes. After this period, excess suspension was forced out of the channels using pressurized air. The reactor was then heated in a furnace at 80°C for 30 minutes to evaporate the remaining water from the slurry, and a furnace at 400°C for 30 minutes to allow calcination of the catalyst layer. After calcination, multiple coating steps could be performed without sacrificing the quality of the previous layer. To increase the layer uniformity and thickness, four coating steps were performed in total, switching the end of the reactor from which the catalyst was injected and the pressurized air was introduced, as well as the surface on which the reactor rested prior to slurry removal.

The catalyst mass per reactor obtained through this process ranged from 161 to 243 mg (~28 – 66 mg per addition step), which corresponds to a specific loading of 2.3 to 3.5 mg/cm^2 of silicon surface and ~6.5 – 9% of total reactor mass. The deposited mass was proportional to the number of addition steps, the slurry solids concentration, and the resting time during deposition. An image of the typical catalyst layer cross-section in the channel is shown in Figure 2d, which shows the accumulation of catalyst in the channel corners due to surface tension effects. The catalyst layer thickness varied from 20 to 70 μm on the top and bottom faces, with a representative image shown as Figure 2e. The catalyst layer was ~10 μm on the side walls, which indicates that the catalyst distribution could be improved with more addition steps where the reactor was held on its side during the resting period. The reactors used in this work contained 229 and 243 mg of catalyst for a total catalyst mass of 471 mg.

Steel manifolds were designed to distribute the fuel and air evenly across the channels without imposing significant additional pressure drop. The manifolds were compression-sealed to the sides of the combustor using Belleville disc springs (Gardener Spring). A soft 99.999% pure aluminum gasket (ACI Alloys and Newcut, inc.) was used to facilitate a gas-tight seal between the steel and the silicon reactors. The manifolds were manufactured using direct metal laser sintering from 17-4 PH stainless steel. The internal structure of the manifold was designed using a CFD simulation to ensure that the flow was evenly distributed without the imposition of significant pressure drop. The flow path widens rapidly away from the combustor until connecting to a 3/8-inch-diameter tube. One downside of the manifold design is the potential for conductive heat losses to dominate the energy balance. The manifold and inlet and outlet tubes were insulated using 1/16-in-thick CeraTex ceramic tape (Mineral Seal Corporation) to minimize this heat loss by extending the length of the temperature gradient. At 136 g, the manifolds dominated the combustor mass. However, there is significant opportunity for weight reduction from the current design with no impact on performance.

Two BiTe-based HZ-2 TE modules were obtained from Hi-Z Technologies, Inc. The modules have a footprint area of 2.9 x 2.9 cm^2, and the reported conversion efficiency is greater than 4.5%. These modules sandwich the combustor, as shown in Figure 1, and are contacted on the other side by an air-cooled heat sink (Aavid Thermalloy). A 1.5-mm-thick graphite layer (GrafTech International) was placed next to the combustor to provide thermal spreading and mechanical compliance, as well as to allow a 36-AWG k-type thermocouple (Omega Engineering) to be placed at the center of the reactor surface (in a small cut in the graphite). On either side of the TE modules, 0.27-mm-thick alumina insulating shims (Hi-Z Technologies) were used to prevent electrical short-circuiting of the TE elements. Thermal paste from Hi-Z technologies was used on all cold interfaces and a high-temperature thermal paste (Epoxy Technologies, Inc.) was used on all hot interfaces. The system was held together by two aluminum clamp plates and four bolts and nuts. The light-weight heat sinks were cooled using an 8 x 8 x 2 cm^3 fan (Delta), which consumed 1.35 W power. The heat sink temperature was measured with self-adhesive k-type thermocouples (Omega Engineering). The system components are shown in Figure 3a, and the assembled system is shown in Figure 3b.

4. Experimental

4.1 Instrumentation and Control

A schematic of the experimental system is shown in Figure 4. The flow of gas from the cylinders was regulated using calibrated mass flow controllers (MKS Instruments and UNIT Instruments), and the distribution of air and of fuel to each of the two reactors was controlled manually with needle valves (Swagelok). Air and fuel streams mixed just before the distribution manifold. A small flow of argon (10.5 sccm) was included in the fuel stream to provide an internal standard for gas composition analysis with a mass spectrometer (Inficon). Pressure measurements were made using an ultra-low-pressure silicon pressure sensor (Honeywell ASDX series). Due to limitations of the sensor, pressure measurements were performed at ambient temperature with air flow. Temperature, pressure, and voltage measurements were recorded with a data acquisition unit (Agilent).

The electrical circuit consisted of the two TE modules, one or more adjustable tubular wirewound resistors (Ohmite) to serve as the "load", and a calibrated shunt resistor (Simpson Electric Co.) to measure the electrical current. The voltage drop across the "load" and across the shunt resistor was measured and recorded by the data acquisition unit. The shunt is calibrated to have a linear response between 0 and 50 mV for current of 0 to 5 A. The two TE modules were connected either in series or in parallel. The power provided to the load was calculated from the product of the measured voltage

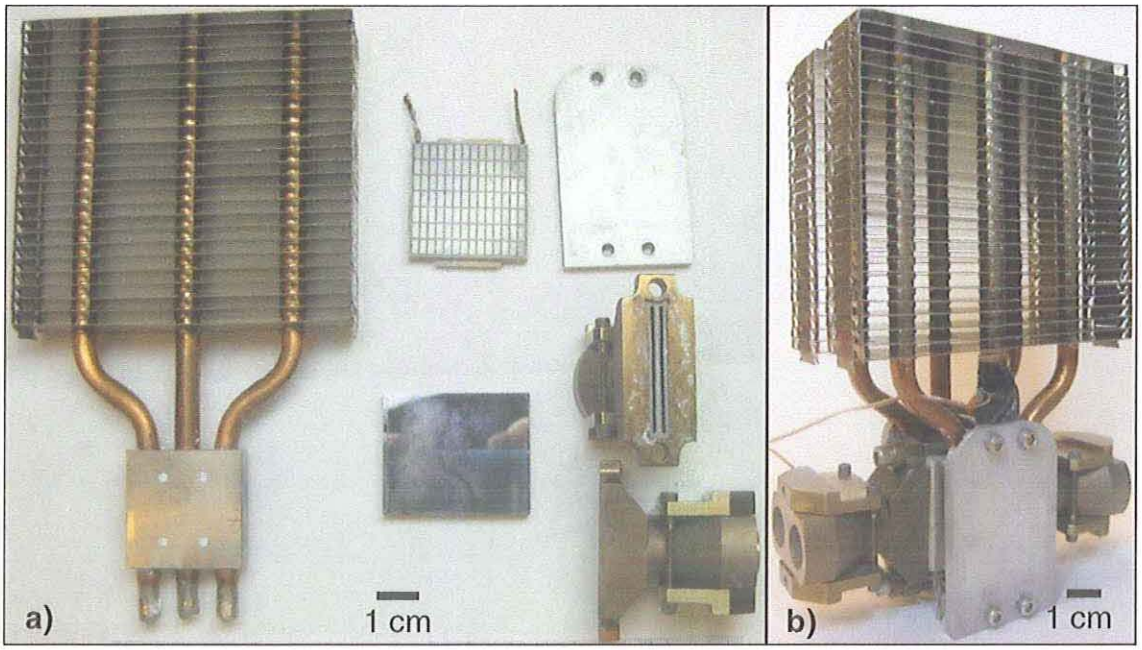

Figure 3: a) System components. Clockwise from top left: heat sink, TE module, clamp plate, gas distribution manifold with aluminum gasket, side view of manifold, and combustor (in center). b) Assembled TE generator.

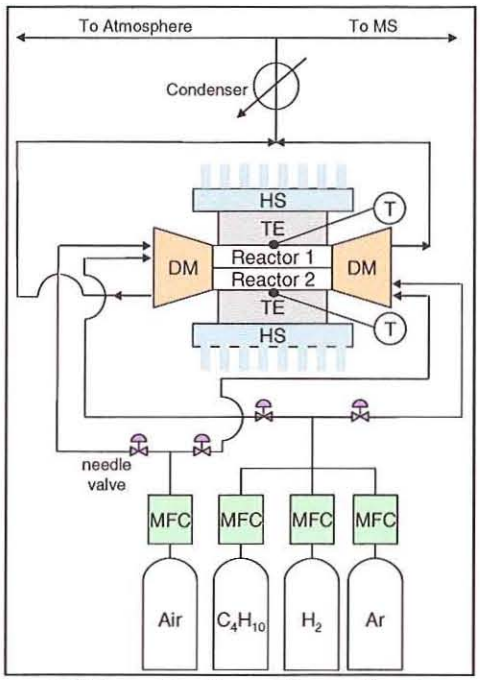

Figure 4: Schematic of experimental system (electrical connections not shown). MFC represents mass flow controllers, DM represents distribution manifold, HS represents heat sink, and "T" surrounded by a circle represents a thermocouple

drop across the load resistor and the current measured by the shunt.

4.2 Experimental Procedure

Hydrogen-assisted catalytic butane combustion (as discussed in [35-37]) was used to achieve reactor ignition, though ignition could also be achieved by electrically heating the inlet tubes while air flowed through the reactor. For the hydrogen-assisted ignition, the lower heating value (LHV) of the ignition-gas mixture was held approximately constant. The initial flow consisted of 4000 sccm of air, 500 sccm of hydrogen (90 W LHV), and 69 sccm of n-butane (137 W LHV), and over time the hydrogen flow was gradually decreased and the butane flow was increased to compensate. The electrical connection to the load resistor was broken during ignition to reduce the rate of heat removal from the combustor and allow for faster start-up.

Once stable butane operation was achieved, the electrical circuit was closed and the system would reach a new stable state. The typical timescale for equilibration between measurements was 10 minutes, though it was dependent on the magnitude of the change in the load resistance (and associated change in the Peltier heat transfer). With the fuel and air flow held constant, the load resistance was changed to determine the response of reactor temperature and power generation to changes in the load. Once the resistance range had been swept, the fuel and air flow was adjusted to vary the combustor temperature.

5. Results and Discussion

5.1 TE Generator Performance

Four different flow rates of butane were used for TE power generation in this system. The lowest flow rate, 106 sccm (209 W LHV), was considered because it was on the stability boundary in terms of autothermal combustion of butane. A higher flow rate, 116 sccm (230 W LHV), was used because it provided a "hot-side" temperature at the TE module (accounting for the thermal resistance of the alumina insulating shim) close to 300°C, which was identified by the manufacturer as a moderately "safe" limit for operation without much damage to the modules. A third flow rate, 111 sccm (220 W LHV), was chosen as an intermediate value between the lowest, barely stable rate and the highest "safe" operation rate.

The fourth and highest butane flow rate, 164 sccm (323 W LHV), was used in a separate system (i.e., duplicate combustor and TE modules) to test the maximum amount of power that could be produced with relaxed temperature constraints. The maximum temperature at the TE module for this butane flow rate was close to the "intermittent operation" temperature limit of 400°C, and would degrade the TE modules over time. There was a known gas leak from the combustor used at this highest flow rate (due to a crack in the silicon) of ~10% of the flow, as determined by measurement of the exhaust flow from a known inlet flow rate.

The TE power generated from the catalytic combustion of butane is shown in Figure 5 as a function of the voltage drop across the load. The conditions at the maximum power point for each flow rate and circuit connection are given in Table 1. In this figure, the power produced with a parallel circuit connection is represented by symbols with solid color, while the power produced with a series circuit connection is represented by gray-filled symbols. The symbol shape represents the flow rate of butane, as listed in the legend.

The two down-arrows indicate the points at which the lowest flow rate was on the border of stability to sustain autothermal butane combustion (the system would be stable with resistances above the load resistance at this point, and unstable with load resistances below). The observed reactor temperatures at these two extinction points were

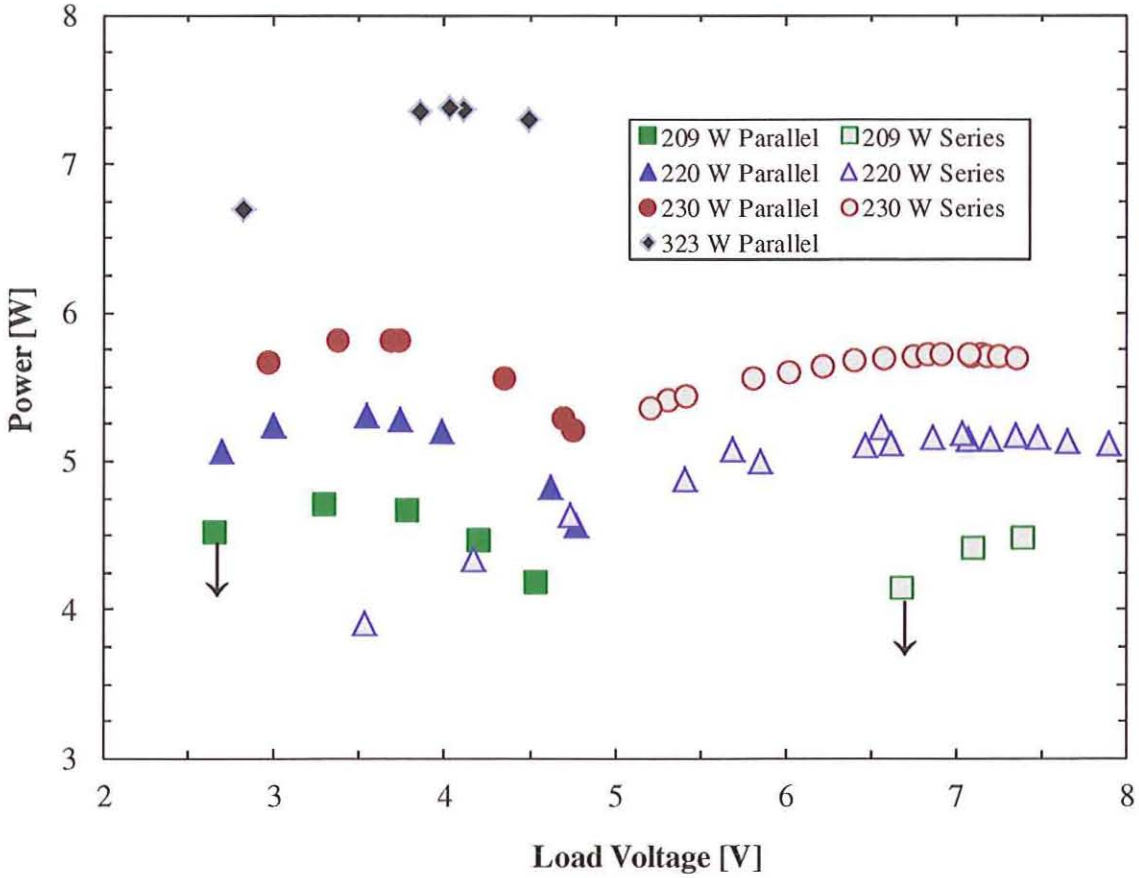

Figure 5: Power provided to the load as a function of load voltage drop, circuit connection and butane flow rate.

similar (268°C for the series circuit and 272°C for the parallel circuit).

The maximum power produced from butane combustion (within the temperature limit for stable operation) was 5.82 W, with an overall chemical-to-electrical conversion efficiency of 2.53% (based on LHV). This performance compares quite favorably with other portable-scale TE power generators found in the literature. The overall conversion efficiency was observed to increase with increased butane flow, and this was in large part related to the increased fuel conversion at higher reactor temperatures, as shown in Figure 6. The butane conversion was nearly complete for the butane flow rate of 116 sccm, which suggests that the conversion efficiency at higher flow rates would be similar. The air equivalence ratio was also slightly higher for the larger butane flow experiments, which led to slightly decreased proportion of heat loss to exhaust enthalpy. A slight air excess was found to produce improved

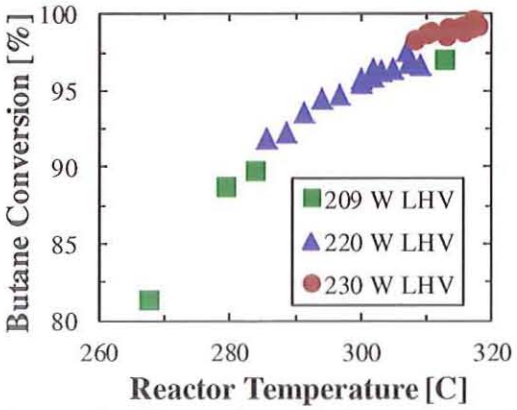

Figure 6: Conversion of butane in the combustor as a function of reactor temperature for the series circuit configuration. The different symbols indicate the flow rate of butane, given in the legend.

Table 1: Maximum power point conditions. The * denotes values obtained from a system with a known leak, such that some portion of the butane may not have passed through the combustor. T_H is the average combustor temperature and T_C is the heat sink temperature.

Butane Flow [W LHV]	Air Equivalence Φ	Circuit Connection	Max. Power [W]	Conversion Efficiency [%]	Voltage at P_{MAX} [V]	Current at P_{MAX} [A]	T_H [C]	T_C [C]
209	0.84	Series	4.49	2.14	7.39	0.61	280	46
220	0.87	Series	5.22	2.38	6.56	0.80	300	51
230	0.89	Series	5.72	2.49	6.83	0.84	314	49
209	0.84	Parallel	4.72	2.25	3.29	1.44	274	44
220	0.85	Parallel	5.31	2.42	3.54	1.50	297	47
230	0.93	Parallel	5.82	2.53	3.73	1.56	312	46
323*	0.96	Parallel	7.37	2.28	4.03	1.83	401	66

performance, but this is likely a result of difficulty with the manual valve-controlled flow distribution.

At the "intermittent operation" temperature limit, the maximum power produced was 7.37 W. The observed conversion efficiency (calculated from the total butane flow provided) of 2.28% for this leaking system was 90% of the maximum conversion efficiency observed at the highest flow rate in the well-sealed system, which corresponds with the independently-estimated leak from the system. This operating condition is not feasible for long-term operation of the TE modules, but it demonstrates the maximum amount of power that could be temporarily generated by the system in response to a spike in demand. This performance also demonstrates the level of performance that could be achieved with TE modules that could perform at slightly higher temperatures, such as encapsulated BiTe-based modules or PbTe-based modules.

Given the maximum observed chemical-to-electrical energy conversion efficiency of 2.53% and the energy density of n-butane (12700 W h kg^{-1}), the maximum energy density which the generator could reach is 321 W h kg^{-1}, which is similar to that of the best lithium-ion cells. The mass of "essential" system components, which includes the combustor (6 g), the gas manifolds and sealing bolts (147 g), the TE modules (28 g), and the heat sinks (159 g), was 340 g. Based on the 5.82 W power produced, and the mass of "essential" system components, the power density of the generator is 17 W kg^{-1}.

5.2 System Analysis

The measured pressure drop through the combustor and manifolds, as a function of air flow rate in liters per minute (lpm), is given in Figure 7 as filled circles. Also shown in this figure (as a solid line) is the calculated pressure drop for laminar air flow through the reactor channels. For the model, the catalyst layer was assumed to be uniform across each side and along the length, with a thickness of 70 μm on top and bottom of the channel and a thickness of 20 μm on each side, which represent the high end of the observed layer thicknesses. The nonlinear response of the measured system pressure drop with flow rate was a result of the flow through the gas distribution manifold, as confirmed by the measured pressure drop through only one manifold (shown as open circles).

Given a highest air flow rate used in the "stable operation" experiments (4056 sccm) and measured pressure drop for the temperature-corrected flow (130 Pa at 9.08 lpm), the minimum flow work required for air pressurization would be 0.01 W. Assuming 10% efficient compression, this would correspond to a parasitic power load for air pressurization of 0.1 W, or less than 2% of the total power produced. This system represents a significant step towards an air-breathing fuel processor with low parasitic power loss for air pressurization.

A heat balance on the combustor was developed from a model of the TE modules presented by Rowe [9], and is represented as equation 1. The heat which entered the combustor consists of the heat of combustion and half of the Joule heating due to current flow through the TE modules (according to equation 5). The heat removed from the combustor in the enthalpy of the exhaust gas is calculated according to equation 2. The heat transfer through the TE modules by thermal conduction and Peltier heat transfer are calculated according to equations 3 and 4, respectively. The heat loss from the combustor to the environment through convection, radiation, and conduction to the fluidic connections are grouped as Q_{system}. The thermal conductivities, Seebeck coefficients, and electrical resistivities of the n- and p-type thermoelectric materials, as well as the

$$Q_{combustion} + \frac{1}{2}Q_{Joule} - Q_{enthalpy} - Q_{conduction} - Q_{Peltier} - Q_{system} = 0 \quad [1]$$

$$Q_{enthalpy} = H_{exhaust}(T_H) - H_{exhaust}(T_C) \quad [2]$$

$$Q_{conduction} = (N+1)\frac{A_e(k_n+k_p)}{L_e}\Delta T_{TE} \quad [3]$$

$$Q_{Peltier} = N(\alpha_p - \alpha_n)T_{H,TE}i \quad [4]$$

$$Q_{Joule} = N\frac{L_e(\rho_p+\rho_n)}{A_e}i^2 \quad [5]$$

area and length of the elements, were provided by the manufacturer.

The heat balance on the reactor was calculated for the conditions of maximum stable power production, where 5.82 W of electrical power were generated at 2.53% efficiency with a parallel circuit connection. The enthalpy loss from the reactor, given the average reactor temperature of 312°C, was 37 W. The conductive heat loss through the TE modules was 100 W, while 2 W were transferred back to the reactor as a result of Joule heating in the TE modules. The Peltier heat transfer from the reactor, given the current of 1.56 A (distributed between the two modules), was 17 W. The heat released in the reactor was 230 W, which leaves 78 W of heat lost to the environment through conduction, convection and radiation. The estimated combustor efficiency (i.e., the fraction of heat released that was transferred to the TE modules) was 51%. It is important to note that these values are very sensitive to the TE material property estimates. However, the predicted TE module conversion efficiency was 5%, which corresponds with the performance predicted by the manufacturer.

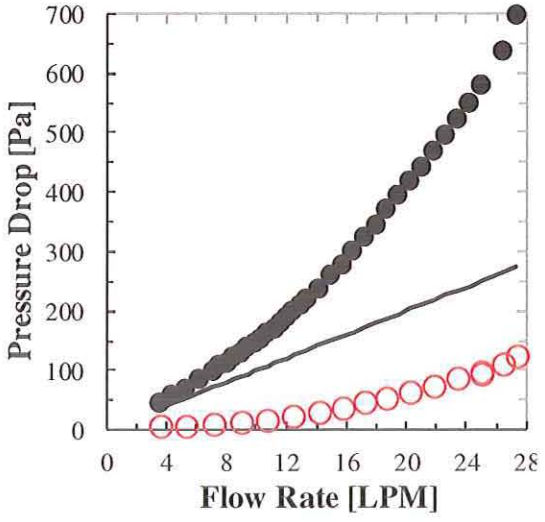

Figure 7: System pressure drop as a function of air flow rate. Filled circles show measured pressure drop through reactor and manifolds. Open circles show measured pressure drop across one manifold. Line shows calculated pressure drop using a laminar flow model of catalyst loaded channels only.

6. Conclusions

A portable-scale thermoelectric power generator was designed, fabricated, and tested. The basis of the system was a mesoscale silicon reactor for the combustion of butane over an alumina-supported platinum catalyst. The system was integrated with commercial bismuth telluride thermoelectric modules to produce 5.82 W of electrical power with a chemical-to-electrical conversion efficiency of 2.53% (based on LHV). The energy and power densities of the demonstrated system were 321 Wh/kg and 17 W/kg, respectively. The pressure drop through the system was 130 Pa for the highest flow rate used, resulting in a parasitic power requirement for air-pressurization of ~0.1 W. The demonstration represents an order-of-magnitude improvement in portable-scale electrical power from thermoelectrics and hydrocarbon fuels, and a notable increase in the conversion efficiency compared with other published works.

7. Acknowledgements

The authors thank MIT Lincoln Laboratory for funding, and Dr. Christopher Vineis, Dr. Todd Mower, and Keith Patterson for their contributions. The authors also thank Walker Chan of MIT for his assistance with assembly of the electrical circuits. This work is sponsored by the Department of the Air Force under Air Force Contract #FA8721-05-C-0002. Opinions, interpretations, conclusions, and recommendations are those of the author and are not necessarily endorsed by the United States Government.

8. References

[1] J.D. Holladay, E.O. Jones, M. Phelps, J. Hu, Journal of Power Sources, 108 (2002) 21-27.

[2] M. Yunt, B. Chachuat, A. Mitsos, P.I. Barton, AIChE Journal, 54 (2008) 1254-1269.

[3] J.-H. Cho, C.S. Lin, C.D. Richards, R.F. Richards, J. Ahn, P.D. Ronney, Proceedings of the Combustion Institute, 32 (2009) 3099-3105.

[4] A. Mehra, Z. Xin, A.A. Ayon, I.A. Waitz, M.A. Schmidt, C.M. Spadaccini, Microelectromechanical Systems, Journal of, 9 (2000) 517-527.
[5] P. Bermel, M. Ghebrebrhan, W. Chan, Y.X. Yeng, M. Araghchini, R. Hamam, C.H. Marton, K.F. Jensen, M. Soljačić, J.D. Joannopoulos, S.G. Johnson, I. Celanovic, Opt. Express, 18 (2010) A314-A334.
[6] J.A. Federici, D.G. Norton, T. Brüggemann, K.W. Voit, E.D. Wetzel, D.G. Vlachos, Journal of Power Sources, 161 (2006) 1469-1478.
[7] S.K. Kamarudin, F. Achmad, W.R.W. Daud, International Journal of Hydrogen Energy, 34 (2009) 6902-6916.
[8] J.D. Holladay, Y. Wang, E. Jones, Chemical Reviews, 104 (2004) 4767-4790.
[9] D.M. Rowe, CRC handbook of thermoelectrics, CRC Press, Boca Raton, FL, 1995.
[10] T. Kajikawa, Journal of Electronic Materials, 38 (2009) 1083-1088.
[11] R. Venkatasubramanian, E. Siivola, T. Colpitts, B. O'Quinn, Nature, 413 (2001) 597-602.
[12] A.L. Cohen, P.D. Ronney, U. Frodis, L. Sitzki, E.H. Meiburg, S. Wussow, in, USA, 2005.
[13] J. Vican, B.F. Gajdeczko, F.L. Dryer, D.L. Milius, I.A. Aksay, R.A. Yetter, Proceedings of the Combustion Institute, 29 (2002) 909-916.
[14] K. Yoshida, S. Tanaka, S. Tomonari, D. Satoh, M. Esashi, Microelectromechanical Systems, Journal of, 15 (2006) 195-203.
[15] D.G. Norton, K.W. Voit, T. Brüggemann, D.G. Vlachos, in: 24th Army Science Conference, Orlando, FL, 2004.
[16] D.G. Norton, E.D. Wetzel, D.G. Vlachos, Industrial & Engineering Chemistry Research, 45 (2005) 76-84.
[17] A.M. Karim, J.A. Federici, D.G. Vlachos, Journal of Power Sources, 179 (2008) 113-120.
[18] S.A. Jacobson, A.H. Epstein, in: The International Symposium on Micro-Mechanical Engineering, 2003.
[19] D. Satoh, S. Tanaka, K. Yoshida, M. Esashi, Sensors and Actuators A: Physical, 119 (2005) 528-536.
[20] L.R. Arana, S.B. Schaevitz, A.J. Franz, M.A. Schmidt, K.F. Jensen, Microelectromechanical Systems, Journal of, 12 (2003) 600-612.
[21] C. Kuei-Sung, et al., Journal of Micromechanics and Microengineering, 15 (2005) S171.
[22] S. Srinivas, A. Dhingra, H. Im, E. Gulari, Applied Catalysis A: General, 274 (2004) 285-293.
[23] B.S. Blackwell, Massachusetts Institute of Technology. Dept. of Chemical Engineering., in, 2008, pp. 174 p.
[24] O.J. Kwon, D.H. Yoon, J.J. Kim, Chemical Engineering Journal, 140 (2008) 466-472.
[25] Y. Suzuki, J. Saito, N. Kasagi, JSME International Journal Series B Fluids and Thermal Engineering, 47 (2004) 522-527.
[26] G. Guan, R. Zapf, G. Kolb, Y. Men, V. Hessel, H. Loewe, J. Ye, R. Zentel, Chemical Communications, (2007) 260-262.
[27] J.Y. Won, H.K. Jun, M.K. Jeon, S.I. Woo, Catalysis Today, 111 (2006) 158-163.
[28] O. Takashi, L. Gwang-Goo, S. Yuji, K. Nobuhide, M. Shin, Journal of Micromechanics and Microengineering, 16 (2006) S198.
[29] J. Zhou, Y. Wang, W. Yang, J. Liu, Z. Wang, K. Cen, International Journal of Hydrogen Energy, 34 (2009) 3535-3545.
[30] G.-B. Chen, C.-P. Chen, C.-Y. Wu, Y.-C. Chao, Applied Catalysis A: General, 332 (2007) 89-97.
[31] N.S. Kaisare, S.R. Deshmukh, D.G. Vlachos, Chemical Engineering Science, 63 (2008) 1098-1116.
[32] A.M. Moreno, B.A. Wilhite, Journal of Power Sources, 195 (2010) 1964-1970.
[33] M.A. Schmidt, Proceedings of the IEEE, 86 (1998) 1575-1585.
[34] A.E.W. Beers, T.A. Nijhuis, F. Kapteijn, J.A. Moulijn, Microporous and Mesoporous Materials, 48 (2001) 279-284.
[35] V. Seshadri, N.S. Kaisare, Combustion and Flame, In Press, Corrected Proof (2010).
[36] B.-J. Zhong, Q.-T. Yang, F. Yang, Combustion and Flame, 157 (2010) 2005-2007.
[37] D.G. Norton, D.G. Vlachos, Proceedings of the Combustion Institute, 30 (2005) 2473-2480.